This article was downloaded by: [Nanjing University]
On: 03 May 2015, At: 21:05
Publisher: Taylor & Francis
Informa Ltd Registered in England and Wales Registered Number: 1072954 Registered office: Mortimer House, 37-41 Mortimer Street, London W1T 3JH, UK



CrossMark
Click for updates

Phase Transitions: A Multinational Journal
Publication details, including instructions for authors and subscription information:
http://www.tandfonline.com/loi/gpht20

Phase diagram of the relaxor ferroelectric (1 - x)$Pb(Mg_{1/3}Nb_{2/3})O_3$+x$PbTiO_3$ revisited: a neutron powder diffraction study of the relaxor skin effect

D. Phelan[ab], E.E. Rodriguez[ac], J. Gao[d], Y. Bing[d], Z.-G. Ye[d], Q. Huang[a], Jinsheng Wen[e], Guangyong Xu[f], C. Stock[g], M. Matsuura[h] & P.M. Gehring[a]

[a] NIST Center for Neutron Research, National Institute of Standards and Technology, Gaithersburg, USA

[b] Materials Science Division, Argonne National Laboratory, Argonne, USA

[c] Department of Chemistry and Biochemistry, University of Maryland, College Park, USA

[d] Department of Chemistry, Simon Fraser University, Burnaby, Canada

[e] School of Physics, Nanjing University, Nanjing, China

[f] Condensed Matter Physics and Materials Science Department, Brookhaven National Laboratory, Upton, USA

[g] School of Physics and Astronomy, University of Edinburgh, Edinburgh, United Kingdom

[h] Institute for Materials Research, Tohoku University, Sendai, Japan

Published online: 19 Jan 2015.

To cite this article: D. Phelan, E.E. Rodriguez, J. Gao, Y. Bing, Z.-G. Ye, Q. Huang, Jinsheng Wen, Guangyong Xu, C. Stock, M. Matsuura & P.M. Gehring (2015) Phase diagram of the relaxor ferroelectric (1 - x)$Pb(Mg_{1/3}Nb_{2/3})O_3$+x$PbTiO_3$ revisited: a neutron powder diffraction study of the relaxor skin effect, Phase Transitions: A Multinational Journal, 88:3, 283-305, DOI: 10.1080/01411594.2014.989226

To link to this article: http://dx.doi.org/10.1080/01411594.2014.989226

PLEASE SCROLL DOWN FOR ARTICLE

Taylor & Francis makes every effort to ensure the accuracy of all the information (the "Content") contained in the publications on our platform. However, Taylor & Francis, our agents, and our licensors make no representations or warranties whatsoever as to the accuracy, completeness, or suitability for any purpose of the Content. Any opinions and views expressed in this publication are the opinions and views of the authors, and are not the views of or endorsed by Taylor & Francis. The accuracy of the Content should not be relied upon and should be independently verified with primary sources of information. Taylor and Francis shall not be liable for any losses, actions, claims, proceedings, demands, costs, expenses, damages, and other liabilities whatsoever or howsoever caused arising directly or indirectly in connection with, in relation to or arising out of the use of the Content.

This article may be used for research, teaching, and private study purposes. Any substantial or systematic reproduction, redistribution, reselling, loan, sub-licensing, systematic supply, or distribution in any form to anyone is expressly forbidden. Terms & Conditions of access and use can be found at http://www.tandfonline.com/page/terms-and-conditions

Downloaded by [Nanjing University] at 21:05 03 May 2015

Phase Transitions, 2015
Vol. 88, No. 3, 283–305, http://dx.doi.org/10.1080/01411594.2014.989226

Taylor & Francis
Taylor & Francis Group

Phase diagram of the relaxor ferroelectric $(1-x)Pb(Mg_{1/3}Nb_{2/3})O_3+xPbTiO_3$ revisited: a neutron powder diffraction study of the relaxor skin effect

D. Phelan[a,b], E.E. Rodriguez[a,c], J. Gao[d], Y. Bing[d], Z.-G. Ye[d], Q. Huang[a], Jinsheng Wen[e], Guangyong Xu[f], C. Stock[g], M. Matsuura[h] and P.M. Gehring[a]*

[a]*NIST Center for Neutron Research, National Institute of Standards and Technology, Gaithersburg, USA;* [b]*Materials Science Division, Argonne National Laboratory, Argonne, USA;* [c]*Department of Chemistry and Biochemistry, University of Maryland, College Park, USA;* [d]*Department of Chemistry, Simon Fraser University, Burnaby, Canada;* [e]*School of Physics, Nanjing University, Nanjing, China;* [f]*Condensed Matter Physics and Materials Science Department, Brookhaven National Laboratory, Upton, USA;* [g]*School of Physics and Astronomy, University of Edinburgh, Edinburgh, United Kingdom;* [h]*Institute for Materials Research, Tohoku University, Sendai, Japan*

(*Received 10 September 2014; accepted 11 November 2014*)

We revisit the phase diagram of the relaxor ferroelectric PMN-*x*PT using neutron powder diffraction to test suggestions that residual oxygen vacancies and/or strain affect the ground state crystal structure. Powdered samples of PMN-*x*PT were prepared with nominal compositions of $x = 0.10$, 0.20, 0.30, and 0.40 and divided into two identical sets, one of which was annealed in air to relieve grinding-induced strain and to promote an ideal oxygen stoichiometry. For a given composition and temperature the same structural phase is observed for each specimen. However, the distortions in all of the annealed samples are smaller than those in the as-prepared samples. Further, the diffraction patterns for $x = 0.10$, 0.20, and 0.30 are best refined using the monoclinic *Cm* space group. By comparing our neutron diffraction results to those obtained on single crystals having similar compositions, we conclude that the relaxor skin effect in PMN-*x*PT vanishes on the Ti-rich side of the morphotropic phase boundary.

Keywords: relaxors; PMN; phase diagram; morphotropic phase boundary; skin effect; neutron diffraction

Downloaded by [Nanjing University] at 21:05 03 May 2015

1. Introduction

Remarkable differences have been reported between X-ray and neutron diffraction measurements of the crystal structures of the complex perovskite (ABO_3) oxides PMN-*x*PT ($(1-x)Pb(Mg_{1/3}Nb_{2/3})O_3+xPbTiO_3$) [1–5] and PZN-*x*PT (Z=Zn).[6–8] These compounds are solid solutions of, respectively, the relaxors PMN and PZN with the conventional soft-mode ferroelectric $PbTiO_3$, and they exhibit the largest piezoelectric coefficients and electromechanical couplings measured to date.[9,10]Because these properties are widely exploited in numerous device applications, [11] PMN-*x*PT and PZN-*x*PT, as well as many other relaxor-based systems, have received a great deal of attention from the scientific community for well over a decade.[12,13] In spite of this, a consensus on the detailed compositional phase diagram of these materials is lacking, a fact that has hampered efforts to achieve a full understanding of the microscopic origin of their exceptional piezoelectric properties.[14] Much of the difficulty in identifying the correct

*Corresponding author. Email: peter.gehring@nist.gov

© 2015 Taylor & Francis

structures and symmetries of the various phases in PMN-xPT and PZN-xPT stems from the fact that they are so pseudosymmetric that different model structures refine to nearly identical agreement factors. Yet there is compelling evidence that this is not the sole reason. The single-crystal neutron diffraction study of PZN-8%PT by Ohwada et al. revealed signs of an unknown 'phase X' at 330 K, well below $T_C \sim 470$ K, that is inconsistent with the expected rhombohedral crystal structure.[15] That finding motivated the synchrotron X-ray study of an unpoled, single crystal of pure PZN by Xu et al., who discovered that the measured structure at 300 K ($T_C \sim 410$ K) varied with X-ray incident energy E_i: for $E_i = 32$ keV a rhombohedrally split 111 Bragg peak is seen, but for $E_i = 67$ keV the same 111 Bragg peak appears as a sharp, resolution-limited singlet.[6] These results are surprising because they contradict previous studies that show that the ground state of PZN is rhombohedral.[16,17] In particular, the results of Lebon et al., obtained on single crystals using 8.9 keV X-rays, indicate that PZN exhibits a fully rhombohedral phase at 300 K.[17] Xu et al. subsequently showed that unpoled single crystals of PZN-xPT with $x = 4.5\%$ and 8%, although clearly rhombohedral at 300 K, yield different values of the lattice constant a and the rhombohedral angle α when measured with low and high-energy X-rays.[8]

A natural explanation for the varied results on PZN-xPT is based on the extreme differences in penetration depths associated with X-rays and neutrons. X-rays with $E_i = 32$ keV have a penetration depth of order 60 μm for PZN and thus preferentially sample the near-surface volume of the crystal. X-rays with $E_i = 67$ keV penetrate over 400 μm and thus probe a region that is more representative of the bulk, at least one that is much less influenced by surface effects. By contrast, neutron penetration depths are typically on the order of 1 cm; neutrons therefore probe the entire crystal volume. The aforementioned discrepancies can be then reconciled by assuming that single crystal PZN-xPT possesses a distinct surface layer, of order 10−50 μm thick, the structure of which differs from that of the crystal interior. This idea has since become known as the 'anomalous skin effect.'[4] Observations of a skin region that is physically distinct from the bulk have also been made in free-standing single crystals of the rare-earth metals Ho [18] and Tb,[19−21] as well as in the perovskite insulator $SrTiO_3$.[22,23] Much more recently a skin effect has been reported for multiferroic $BiFeO_3$.[24] However, in none of these cases is the skin both macroscopically large (≥1 μm) and present over a temperature range spanning hundreds of degrees Kelvin as it appears to be in relaxors. Independent support for a skin effect in relaxors is seen in the neutron powder diffraction measurements of Fujishiro et al., who concluded that the rhombohedral phase in PZN develops gradually on cooling yet spans less than half the entire crystal at room temperature, which is more than 100 K below T_C.[25] In addition, single crystal neutron diffraction measurements on PZN by Stock et al. show no clear evidence of a rhombohedral distortion.[26] These results notwithstanding, the existence of a skin effect in PZN-xPT has been strongly challenged by Kisi et al. [27,28] and Forrester et al. [29] based on extensive neutron time-of-flight powder and single crystal diffraction measurements made on unpoled single crystals at 300 and 4.2 K. In all cases, an $R3m$ ground state is observed. These authors concluded that the X-phase observations of Xu et al. were the result of an unusual 'rhombohedral domain size and population gradient within the crystals sampled by the small X-ray beam.' The skin effect for the PZN-xPT system is therefore currently controversial.

A skin effect has also been reported in PMN-xPT, and in this case the effect does not appear to be in doubt. Neutron scattering measurements of the 111 and 220 Bragg peaks of a single-crystal of PMN-10%PT, which were made using a perfect single crystal Ge

Downloaded by [Nanjing University] at 21:05 03 May 2015

Downloaded by [Nanjing University] at 21:05 03 May 2015

analyzer to obtain extremely high wave-vector (Q) resolution, show that both peaks are singlets down to 10 K,[1] far below the generally accepted cubic-to-rhombohedral transition temperature T_C =285 K. Subsequent neutron scattering studies were conducted on single crystals of PMN-20%PT and PMN-27%PT by Xu et al. to determine at what Ti concentration x a bulk rhombohedral ground state is finally established.[30] For PMN-20%PT, the 220 Bragg peak is also a singlet at 50 K, but it is much broader than it is in the cubic phase at 400 K, and it is well described by a single Lorentzian peak profile. For PMN-27%PT, the 220 Bragg peak splits below $T_C \sim 375$ K, which is consistent with a transition to a rhombohedral phase, but the individual peak widths are much broader than the instrumental Q-resolution; thus a long-range ordered rhombohedral phase is not present. These results are at odds with the neutron and X-ray powder diffraction study of Dkhil et al. on PMN-10%PT [31] and with the synchrotron powder diffraction study of Ye et al. on ceramic samples of PMN-xPT in which an $R3m$ rhombohedral ground state was reported for compositions as low as $x = 0.05$.[32] The case of pure PMN ($x = 0$) is an interesting one inasmuch as both neutron and X-ray scattering measurements agree that no macroscopic deviation from cubic symmetry occurs down to temperatures as low as 5 K.[33,34] However neutron residual stress measurements made on a large (9.3 cc) single crystal of pure PMN conclusively demonstrate the presence of a substantial near-surface variation in the lattice spacing (strain) over a macroscopic length scale of order 100 μm at room temperature; by comparison, an identical measurement found no such anomaly in a large single crystal of germanium.[3] This result implies that a related skin effect exists even for PMN.

Because the origin of the anomalous skin effect is unknown, we have reinvestigated the phase diagram of PMN-xPT using neutron powder diffraction to test suggestions that defects in the oxygen stoichiometry and/or strain introduced from grinding might play a role in producing this phenomenon. Additional motivation for this study stems from the recent conjecture by Singh et al. that compositions of PMN-xPT located on the Ti-poor side of the morphotropic phase boundary (MPB) are not rhombohedral ($R3m$), as widely believed, but instead exhibit a ground state monoclinic structure for $x \leq 0.30$.[35] To this end, two identical sets of PMN-xPT powders were prepared, only one of which was annealed in air after having been ground. Each set contains four compositions spanning the region between Ti-poor, nominally rhombohedral phases and the MPB, where the piezoelectric properties are largest. Neutron powder diffraction measurements were carried out with high Q-resolution on both sets. For a given composition x and temperature T, the same symmetry is observed in each set, which suggests that the effects of strain and oxygen vacancies on the structures of as-prepared samples are minimal. The diffraction patterns for the as-prepared and annealed samples with compositions $x = 0.10$, 0.20, and 0.30 are best refined using the monoclinic Cm space group. As these findings are inconsistent with neutron diffraction measurements on large single crystal having similar compositions ($x = 0.10$, 0.20, and 0.27), which show no evidence of any long-range ordered structural distortion,[1,2] they support the presence of a skin effect in PMN-xPT for which externally induced strain and oxygen vacancies are not relevant to its origin. We suggest that the data presented here are consistent with a skin effect that is instead a result of the strong random electric fields (REFs) generated by the random mixture of Mn^{2+}, Nb^{5+}, and Ti^{4+} cations on the perovskite B-site. This idea was first suggested by Stock et al. [26,36] because of the close analogy to the skin effect observed in the random-field Ising antiferromagnet $Mn_{0.5}Zn_{0.5}F_2$,[37] and subsequently by Cowley et al. [13]

Downloaded by [Nanjing University] at 21:05 03 May 2015

2. Experimental details

Two sets of PMN-xPT powder samples with compositions $x = 0.10$, 0.20, 0.30, and 0.40 were synthesized using the two-step columbite precursor method. In the first step, a mixture of Nb_2O_5 (99.9%) and MgO (99.95%) containing a 0.9 mass% excess of MgO over the 1:1 stoichiometric ratio was thoroughly ground in ethanol and cold-pressed into pellets. Excess MgO was added to compensate for the thermal weight loss incurred at high temperature as determined from a DTA/TG analysis. The pellets were calcined at 1373 K for 12 h to form the pure columbite phase $MgNb_2O_6$. In the second step, the ground precursor powder was mixed with PbO (99.99%) and TiO_2 (99.9%) according to the stoichiometry of each composition. An excess of 2 mass% PbO was added to compensate for the loss incurred during the subsequent calcining and sintering. The mixture of each composition was thoroughly ground and then calcined at 1170−1220 K for 4−8 h to form the perovskite phase. The calcined powders were reground and cold-pressed into pellets, which were then sintered at 1500 K for 4 h in a sealed alumina crucible to form ceramics. These pellets were crushed, ground into powders, and divided into two sets. The first set of powders produced in this manner will be referred to 'as-prepared' throughout the rest of this manuscript. The second set of powders, henceforth referred to as 'annealed,' were subsequently annealed in air at 873 K for 2 h to relieve any internal strains induced by grinding that might affect the phase symmetry and also to ensure optimal oxygen stoichiometry. X-ray powder diffraction analysis confirmed that all samples exhibit a pure perovskite phase.

All neutron diffraction patterns reported here were measured on the BT-1 powder diffractometer located at the NIST Center for Neutron Research (NCNR).[38] Approximately 5 g of each composition were loaded into a cylindrical vanadium can (inner diameter = 9.2 mm) inside a dry helium-filled glove box, sealed using an indium seal (for temperatures at 300 K and below), leak tested, and then mounted inside a closed-cycle ^{4}He-refrigerator. Powder patterns were collected at 10 K for a period of 12 h using a fixed incident neutron wavelength of 1.5403 Å supplied by a Cu(311) monochromator. The data for each pattern span the angular range $3° \leq 2\theta \leq 157°$ in steps of 0.05°, which converts to $0.21\ \text{Å}^{-1} \leq Q \leq 7.99\ \text{Å}^{-1}$, where Q is the scattering vector or wave vector. Two additional powder patterns were collected from the PMN-20%PT samples at an incident wavelength of 1.1968 Å supplied by a Ge(733) monochromator, which provides better Q-resolution for wave vectors $Q \geq 6.5\text{Å}^{-1}$ and a substantially larger Q-range of $0.27\ \text{Å}^{-1} \leq Q \leq 10.29\ \text{Å}^{-1}$. In all cases, the horizontal beam collimations were 15′-M-20′-S-7′-D (M = monochromator, S = sample, D = detector). The temperature dependence of the 111 Bragg peak for each of the two PMN-20%PT samples was also studied on the BT-9 thermal neutron triple-axis spectrometer, located at the NCNR, at a wavelength of 2.3590 Å ($E_f = 14.7$ meV) using vertically focused PG(002) crystals as monochromator and analyzer and horizontal beam collimations of 15′-M-20′-S-10′-A-10′-D (A = analyzer).

Rietveld refinements were performed using the General Structure Analysis System (GSAS) suite of programs [39] and the EXPGUI graphical user interface to GSAS.[40] The lattice parameters, atomic positions, peak profile coefficients, and atomic displacement parameters were refined along with a shifted Tchebychev background function, scaling factor, and the zero offset of the scattering angle 2θ. In all cases, the stoichiometry (i. e. the occupancies for Mg, Nb, and Ti) was fixed. Further details regarding the choices of peak profile and displacement parameters are given in the next section. The subscript 'pc' is used henceforth to refer to the primitive cubic unit cell containing only one perovskite formula unit ($a_{pc} \approx 4.03$ Å), while the subscript 'r' is used to refer to indexing based on the $R3m$ space group with rhombohedral axes. The subscript 't' is used to refer to

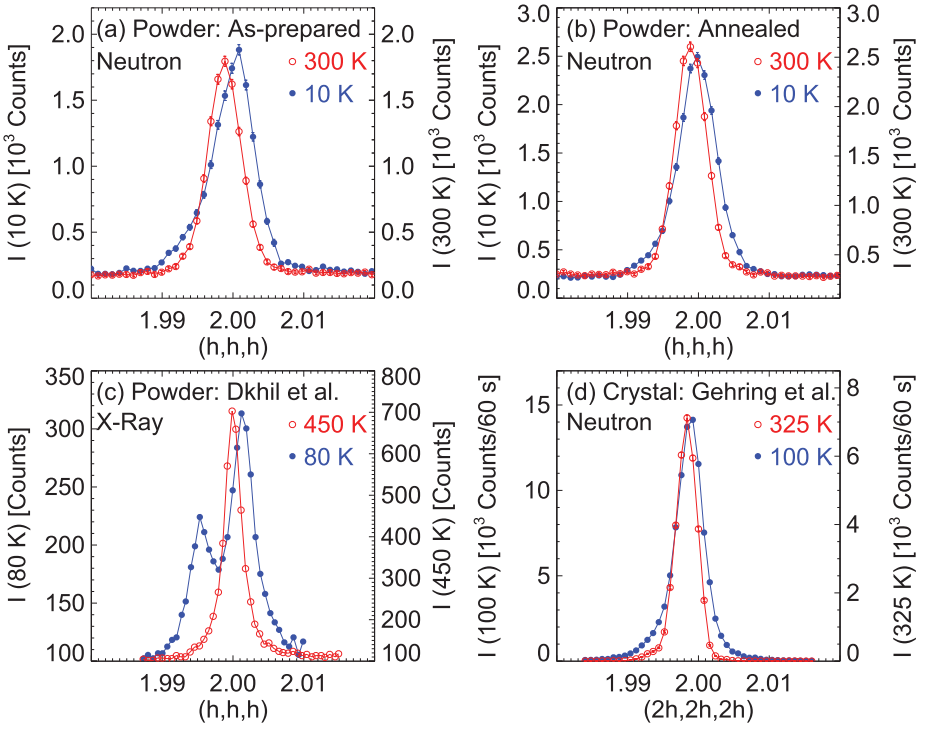


Figure 1. Comparison of the 222_{pc} Bragg peak profiles measured with neutron and X-ray scattering methods for PMN-10%PT. The neutron profiles for the (a) as-prepared and (b) annealed powder samples are shown at 10 K (blue) and 300 K (red). (c) The X-ray powder profile is shown at 80 K (blue) and 450 K (red) (from Dkhil et al. [31]). (d) The 111_{pc} peak profile for single crystal PMN-10%PT at 100 K (blue) and 325 K (red) (from Gehring et al. [1]) The x-axis has been multiplied by a factor of 2 to allow for direct comparison to the other profiles. Error bars represent a statistical uncertainty of $\pm 1\sigma$ for the measured intensities.

Downloaded by [Nanjing University] at 21:05 03 May 2015

indexing based on the *P*4*mm* space group. In Figures 1, 4, and 6, the horizontal scales are given in reciprocal lattice units (rlu), where 1 rlu$= 2\pi/a = 1.56$ Å. In all figures, the error bars represent a statistical uncertainty of one standard deviation ($\pm 1\sigma$) for the measured intensities or for the values of the fitting parameters.

3. Results and discussion

3.1. Structure of PMN-10%PT

In 2001, Dkhil et al. carried out a combined neutron and X-ray diffraction study of powdered and single crystal PMN and PMN-10%PT.[31] Noting that unusually large values of the isotropic thermal displacement parameters for oxygen (B_O) and lead (B_{Pb}) had been reported in pure PMN,[34] which are generally attributed to the presence of local, disordered cation displacements, they refined their neutron powder diffraction data on PMN-10%PT (measured at 80 K) using a model with *R*3*m* symmetry that included disordered shifts of the Pb cation along $<2\bar{1}\bar{1}>$ that succeeded in reducing the size of B_{Pb} from 2.24 Å^2 to a more normal value of 0.67 Å^2.[31] This model crystal structure is interesting because it produces a symmetry that is rhombohedral globally but monoclinic

Downloaded by [Nanjing University] at 21:05 03 May 2015

locally. The idea of a local monoclinic symmetry was actually first used by Corker et al. to describe the structure of PZT.[41] In 2006, Singh et al. used this model to refine neutron powder diffraction data on PMN-25%PT.[42] This produced reasonable agreement with the diffraction data measured at 300 K. However, Singh et al. obtained statistically better refinements of their data measured at 80 K using the M_B-type monoclinic phase (space group *Cm*) in which the components of the polarization $\vec{P}$ are such that $P_x = P_y \geq P_z$. On this basis, they speculated that the ground state structures of all PMN-*x*PT compositions with $x \leq 0.30$ are actually monoclinic *Cm*.[35] The disparate conclusions reached from the powder diffraction studies of Dkhil et al. and Singh et al. as well as those of the synchrotron powder diffraction study of Ye et al. indicate that a consensus on the crystal structure of PMN-*x*PT is lacking. Furthermore, the results of all powder diffraction studies conflict with the high-resolution, single-crystal, neutron diffraction measurements on PMN-10%PT by Gehring et al. [1] and on PMN-20%PT and PMN-27%PT by Xu et al. [2] in which *no* measurable splittings were observed for PMN-10%PT or PMN-20%PT for either the 111_{pc} or the 220_{pc} Bragg peaks, thus implying an average cubic structure for both compounds.

We measured neutron diffraction patterns for the as-prepared and annealed PMN-10%PT powder samples at 300 and 10 K. During all refinements, the stoichiometry was fixed. In particular, the *B*-site occupancies were fixed at 30% Mg, 60% Nb, and 10% Ti for both samples. We used isotropic thermal parameters, which in the case of the *B*-site cations were constrained to be equal, and a conventional variation of a pseudo-Voigt function (CW profile type 3 in GSAS [39]). In addition, the following coefficients were allowed to float: U, V, and W, which control the width of the Gaussian component; LX and LY, which describe the Lorentzian components due to particle-size and strain broadening, respectively; and an asymmetry parameter. The 300 K data were refined using the $Pm\bar{3}m$ space group, and the resulting values of χ^2 and the weighted profile R-factor (R_{wp}) values for the as-prepared and annealed samples were 1.25 (6.80%) and 1.53 (6.19%), respectively, indicating a satisfactory refinement. It is interesting that the annealed sample yields a measurably worse value of χ^2 than does the as-prepared sample.

At 10 K, a broadening of a number of Bragg peaks is evident, which is consistent with a transition to lower symmetry. In particular, the 222_{pc} Bragg peak broadens asymmetrically on cooling and develops a low-angle shoulder at 10 K. This is shown in Figure 1 for the (a) as-prepared and (b) annealed samples. We note that the intensity of this low-angle shoulder is weaker for the annealed sample, and in both cases it is *much* weaker than that observed with X-rays (also on a powder sample) by Dkhil et al. at 80 K, [31] the data for which reveal a clearly split peak as shown in panel (c) of Figure 1.

Rietveld refinements of the 10 K data were carried out using the space groups $Pm\bar{3}m$, *R*3*m*, *P*4*mm*, *Amm*2, *Cm*, and *Pm* using the same protocols used for the 300 K data. Under these conditions, the best refinements were achieved with the *Cm* space group for both as-prepared and annealed samples. The resultant χ^2 and weighted profile R-factors (R_{wp}) are listed in Table 1. Refinements of the as-prepared sample using anisotropic thermal parameters for the lead cation yielded only a negligible improvement in χ^2 from 1.130 to 1.124 using the *Cm* space group and from 1.333 to 1.203 using *R*3*m* space group. We note that the Pb thermal parameters are quite large ($B \approx 2.85$ Å^2), but of the same order as that obtained by Dkhil at 80 K with the perpendicular shifts turned off. [31] In addition, particle sizes of 0.6 μm ± 0.3 μm for the as-prepared sample and 1.0 μm ± 0.5 μm for the annealed sample were obtained for the *Cm* refinement; these values increased slightly (0.9 μm ± 0.4 μm and 1.2 μm ± 0.6 μm) for the $Pm\bar{3}m$ refinement. Based on these values, we conclude that the refined particle sizes of our powder samples exceed the critical size of ≈ 0.4 μm, determined by Carreaud et al., below which it was found that the

Table 1. χ^2 (R_{wp}) for refinements of PMN-10%PT at 10 K.

	$Pm\bar{3}m$ (cubic)	R3m (rhombohedral)	P4mm (tetragonal)	Amm2 (orthorhombic)	Cm (monoclinic)	Pm (monoclinic)
As-prepared	4.33 (11.98)	1.30 (6.55)	2.34 (8.78)	1.46 (6.95)	1.13 (6.10)	1.53 (7.11)
Annealed	4.69 (11.52)	1.95 (7.42)	2.57 (8.52)	1.92 (7.36)	1.72 (6.99)	1.98 (7.49)

structure of PMN-20%PT at room temperature evolves with decreasing particle size from monoclinic M_B to M_A ($P_x = P_y < P_z$) and then eventually to rhombohedral near a particle size of 0.2 μm.[43] Figure 2 shows the 10 K diffraction pattern and difference plot for the as-prepared sample refined under *Cm* symmetry.

Reflections of the form $h00_{pc}$ split into doublets under *Cm* but remain singlets under *R*3*m*, thus they can be used to help distinguish between these two space groups. Figure 3 provides a plot of the values of the Gaussian FWHM (full-width at half-maximum) of several $h00_{pc}$ reflections measured at 300 K (open red symbols) and 10 K (solid blue symbols) as a function of wave vector *Q*. The instrumental resolution is shown for comparison as a solid black line. Although the widths of 100_{pc} and 200_{pc} are nearly temperature independent, the 300_{pc}, 400_{pc}, and 500_{pc} peaks for both samples clearly broaden at 10 K. In principle, one expects peak splittings to increase with *Q*; as such, these broadenings lend credence to the *Cm* model, although this conclusion is somewhat tempered by the lack of a measurable change in the widths of 100_{pc} and 200_{pc}. To gain further insight, we performed a Le Bail fit, which is a refinement in which the peak intensities are optimized without the constraint of a structural model.[44] For the as-prepared powder sample, the resulting values of χ^2 (R_{wp}) for refinements under *R*3*m* and *Cm* are, respectively, 1.17 (6.13%) and 1.07 (5.86%). Thus the monoclinic model proposed by Singh et al. appears to be favored by our refinements for PMN-10%PT.

The refinements discussed above allowed for the possibility of an isotropic strain in the U and Y components of the profile function. Subsequent refinements implemented a different profile function (CW profile type 4 in GSAS) that includes anisotropic strain

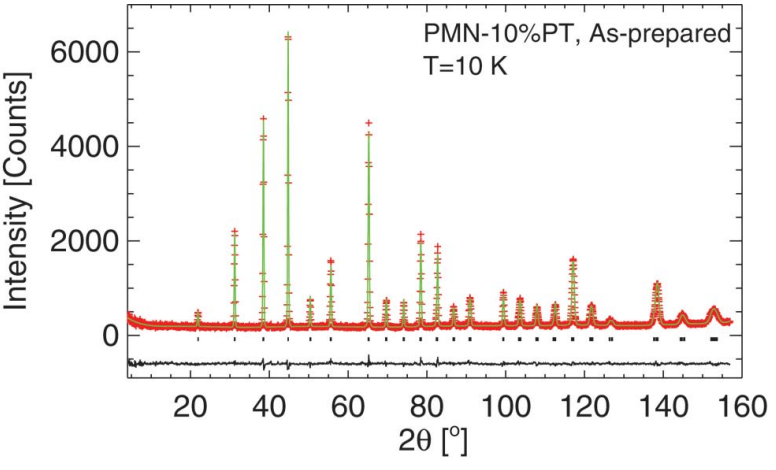


Figure 2. Measured (red +) and calculated (solid green line) neutron diffraction pattern for as-prepared PMN-10%PT at 10 K using the *Cm* space group with $\lambda = 1.5403$ Å. Bragg peak locations are indicated using vertical tick marks, and the difference curve is shown at the bottom.

Downloaded by [Nanjing University] at 21:05 03 May 2015

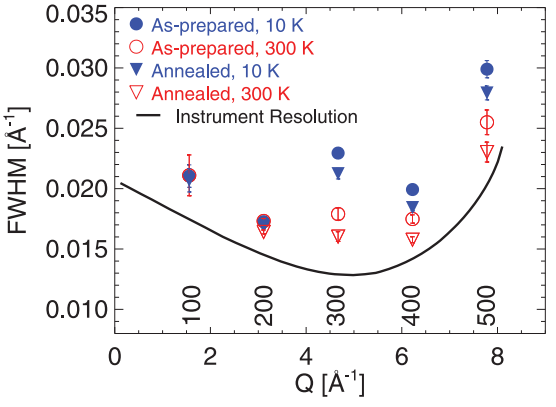


Figure 3. Plot of the FWHM of $h00_{pc}$ Bragg peaks as a function of Q. The instrument resolution comes from the BT-1 website, www.ncnr.nist.gov/instruments/bt1/.

Downloaded by [Nanjing University] at 21:05 03 May 2015

[45] to determine if this would improve the values of χ^2 for $R3m$. While χ^2 for such refinements did decrease from 1.948 to 1.836 for the annealed sample, and from 1.299 to 1.286 for the as-prepared sample, the agreement of the $R3m$ model with anisotropic strain was still not as good as that of Cm with isotropic strain. We did not attempt any refinements using an anisotropic profile function with space group Cm because the effect of doing so has already been studied by Singh et al., and they found that including anisotropic strain does not significantly improve the refinement of a PMN-xPT powder sample with $x = 0.25$.[35]

As mentioned earlier, Dkhil et al. were able to improve their refinement of the $R3m$ phase for PMN-10%PT, while also reducing the size of the thermal factor, by moving the Pb atom off of its special position.[31] A similar improvement in agreement was reported for refinements of PMN-25%PT by Singh et al. by including local Pb displacements along $< 100 >_{pc}$ in addition to those along $< 111 >_{pc}$ allowed by the rhombohedral symmetry.[42] Using the rhombohedral axes of the $R3m$ space group, the Pb atom is located at the 1a site (x,x,x). To investigate the effect of local Pb displacements along $< 100 >_{pc}$, the site symmetry was reduced to 3b, which generates Pb atoms at (x,x,z), (x,z,x), and (z,x,x), and the occupancy was changed to $\frac{1}{3}$ to account for the two extra atoms. Using isotropic thermal parameters and isotropic strain, this improved the χ^2 of the refinements from 1.948 to 1.847 for the annealed sample and from 1.299 to 1.205 for the as-prepared sample. Again, consistent with the findings of Singh et al., this improved agreement still does not match that for Cm.

Comparing Figure 1(a) and 1(b), it is evident that the 222_{pc} Bragg peak of the as-prepared sample is more asymmetric at 10 K than is that for the annealed sample. The degree of the associated distortion is readily quantified by refinements under $R3m$ and Cm symmetry through the values of α and β, respectively, both of which are identically 90° for the cubic structure. The refined values of α and β for both samples at 10 K are given in Table 2, and it can be seen that, independent of the choice of symmetry, the as-prepared sample deviates more from 90° than does the annealed sample. This analysis shows that the process of annealing after grinding affects the structure by slightly reducing the size of the distortion. This is not unexpected as annealing should reduce any residual lattice strains introduced during the final process of grinding the cold-pressed ceramic pellets into powders.

The lineshape of the 222_{pc} Bragg peak measured with X-rays by Dkhil et al. for their PMN-10%PT sample is shown in Figure 1(c) at 80 K and 450 K.[31] A simple

Table 2. Refined values of α ($R3m$) and β (Cm) for PMN-10%PT.

	$\alpha(^\circ)$	$\beta(^\circ)$
As-prepared	89.871(1)	90.173(4)
Annealed	89.902(1)	90.131(4)

comparison of the cubic phase profiles (red data points) shown in panels (c) and (a), respectively, shows that the X-ray Q-resolution is considerably better than that for the BT1 diffractometer. Furthermore, the 222_{pc} peak is clearly split at 80 K, which indicates unambiguously that a phase transition has occurred. A refined value of $\alpha = 89.87(1)$ for the $R3m$ space group was reported at 80 K, which, for the purposes of comparison, is essentially identical to the refined value of α for our as-prepared powder sample at 10 K. Because the temperature dependence of α, shown in Figure 1 of [31], is roughly flat below $\approx$ 150 K, we conclude that the crystal structures of our as-prepared sample and that of Dkhil et al. are consistent with one another.

The neutron diffraction data shown in Figure 1(d) were obtained from radial scans through the 111_{pc} Bragg peak of a 2.65 g single crystal of PMN-10%PT measured with extremely high Q-resolution (1.8×10^{-3} rlu FWHM) provided by a perfect single crystal Ge analyzer,[46] as reported in [1] The radial scans are shown at 325 and 100 K. A narrow lineshape is observed at 325 K, in what is indisputably the cubic phase, and the corresponding linewidth is comparable to that of the X-ray profile shown in Figure 1(c). Remarkably, when the same scan was repeated at 100 K, which is nearly 200 K below T_C, no splitting was observed. It was thus concluded that the PMN-10%PT single crystal exhibited a highly strained, metrically cubic, ground-state structure. We elaborate further on these single crystal measurements below.

If one assumes that the 100 K structure of the PMN-10%PT single crystal is $R3m$, then the intensity ratio of the $11\overline{1}_r$ peak to the 111_r peak should be approximately 3.55:1 given the multiplicities and the structure factors determined from the Rietveld refinement of the as-prepared PMN-10%PT powder. (This argument also applies if the space group is Cm because the lattice parameters of Cm are extremely pseudo-rhombohedral.) Knowing this intensity ratio, the lineshape expected for the rhombohedral structure can be calculated assuming an equal proportion of all domain types. When doing this calculation, it is important to note that the linewidths of radial scans measured using this particular high Q-resolution configuration are coupled to the mosaic of the crystal. The reason for this is that a highly oriented pyrolytic graphite (HOPG) crystal was used as monochromator while a Ge single crystal was used as analyzer; such an asymmetric instrumental configuration causes the major and minor axes of the elastic resolution ellipse to rotate so that they no longer coincide with the radial and transverse directions in reciprocal space. Thus as the crystal was cooled and the mosaic width broadened the radial linewidth also broadened. The radial linewidth was calculated from the measured mosaic and the other instrumental parameters, and this was used to generate the radial scan profile through the 111_{pc} Bragg peak shown by the solid line in Figure 4(a). The measured scan at 100 K is clearly inconsistent with this simulated profile. Regardless of whether the crystal structure is rhombohedral or cubic, a lineshape much broader than the resolution limit is required to fit the data. This indicates that there is a substantial amount of strain broadening at low temperature. Unfortunately this strain broadening makes it difficult to identify the correct structure because it interferes with the presence of any potential splitting.

Downloaded by [Nanjing University] at 21:05 03 May 2015

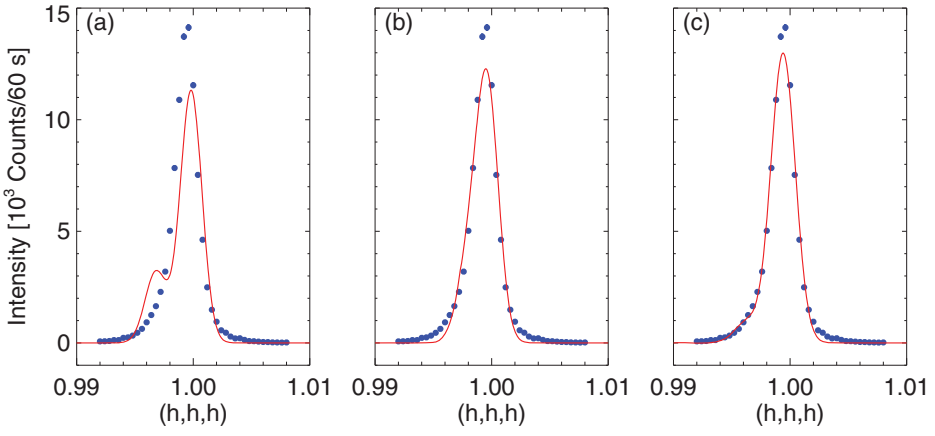


Figure 4. Radial scan (neutron) through the 111_{pc} Bragg peak of single crystal PMN-10%PT at 100 K (blue dots). (a) The anticipated lineshape of a domain-averaged radial scan based on the rhombohedral model (red line). (b) A two-Gaussian fit in which the peak widths are constrained to be equal and allowed to float, *and* the ratio of the two peak intensities is constrained to be 3.55:1 (red line). (c) A two-Gaussian fit in which only the peak widths are constrained to be equal (red line).

A close inspection of the radial scan at 100 K in Figure 1(d) reveals that the peak profile is not quite symmetric. Likewise, the scan measured in the cubic phase at 325 K is also slightly asymmetric. This could be explained by a spatial gradient of the crystal lattice constant. Such a situation has already been documented using neutron diffraction by Conlon et al. on a large single crystal of PMN.[3] However, the asymmetry is more pronounced at 100 K than 325 K. Therefore, the 111_{pc} peak profile at 100 K was fit using a two-Gaussian model to test the possibility that the broadening is actually the result of a weak rhombohedral splitting of the peak into a doublet. Two such fits were performed. For the first, shown in Figure 4(b), the ratio of the peak intensity of the $11\overline{1}_r$ peak to the 111_r peak was forced to be 3.55:1 as determined by the structure factor calculation from the powder refinement. The two peaks were also constrained to have the same linewidth, but the linewidth was allowed to vary to account for possible strain broadening. This model still does not fit the observed intensity very well, which indicates that the data are inconsistent with a domain-averaged rhombohedral structure.

For the second fit, shown in Figure 4(c), the same model was used. However, no constraint was placed on the ratio of the integrated peak intensities. This model describes the data much better, although it still does not capture all of the peak intensity or the weak scattering present on the high-Q side of the Bragg peak. The fitted value of α for this model is 89.866(10)°, which is close to the value observed in the powder neutron diffraction experiment. However the ratio of the peak intensities is 13.8:1, which is substantially larger than that expected for such a large single crystal. This indicates that the symmetry of the structure could be consistent with the rhombohedral symmetry, but only if there were a very uneven distribution of domains. This is extremely unlikely for such a large (2.65 g) single crystal sample.

Another interesting aspect of the single crystal measurement is the dramatic change in the 111_{pc} peak intensity evident in Figure 1(d); the peak intensity increases nearly two-fold on cooling from 325 to 100 K. Data were collected for temperatures between 50 and 500 K, and the intensity of the radial scan was summed over a range of wave vectors from $\vec{Q} = (0.992, 0.992, 0.992)_{pc}$ to $\vec{Q} = (1.0076, 1.0076, 1.0076)_{pc}$. The results are shown in Figure 5, and it is clear that the intensity increases enormously, albeit gradually, as the

Downloaded by [Nanjing University] at 21:05 03 May 2015

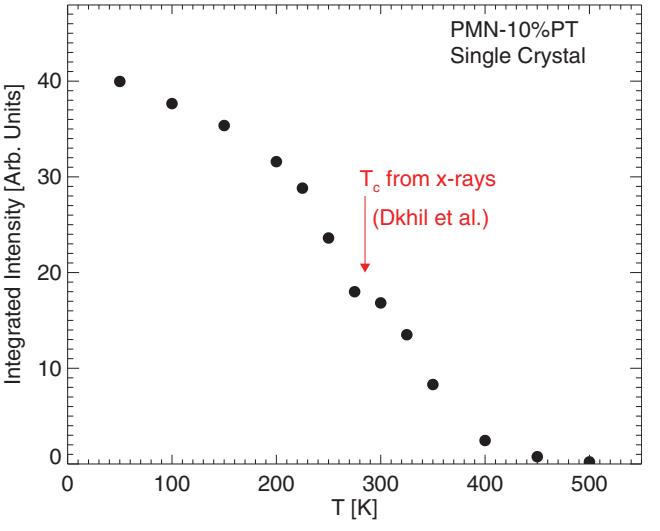


Figure 5. Temperature dependence of the numerically integrated neutron scattering intensity from radial scans through the 111_{pc} Bragg peak of single crystal PMN-10%PT. The 285 K Curie temperature identified by Dkhil et al. [31] is marked by the red arrow.

temperature is lowered. An increase of this magnitude cannot be explained by a change in the structure factor of a fundamental Bragg peak such as 111, and it is many times beyond what one would expect from the Debye−Waller factor. Instead, the increase must be related to a release of extinction. This has two possible origins − either a macroscopic phase transition or the development of significant strain due to the formation of polar nanoregions or local atomic displacements. The first possibility is inconsistent with the fact that the release of extinction begins just above 400 K, which is far above the critical temperature $T_C = 285$ K identified in the X-ray diffraction study of PMN-10%PT.[31] In addition, the structural phase transitions observed in Ti-poor compositions of PMN-*x*PT are first-order, [31,32] whereas the change in intensity shown in Figure 5 takes place slowly on cooling. On the other hand, the *elastic* diffuse scattering in pure PMN, which is commonly believed to arise from local polar displacements, appears around 410 K and exhibits a similarly broad temperature dependence.[47,48] It is therefore tempting to attribute the release of extinction to the condensation and subsequent growth of polar nanoregions. While this idea satisfactorily explains the basic shape of the temperature profile in Figure 5, it does not explain the obvious inflection point located below 300 K. Because this occurs so close to the critical temperature $T_C = 285$ K, we speculate that this reflects the onset of the release of extinction driven by the cubic-to-rhombohedral phase transition observed by Dkhil et al. in the skin region. In this sense, the data in Figure 5 reveal a rather unique case of extinction release that, on cooling, is first driven by strain and then by a macroscopic phase transition, which is limited to the near-surface region of the crystal.

Table 3. χ^2 (R_{wp}) for refinements of PMN-20%PT at 10 K.

	$Pm\bar{3}m$ (cubic)	R3m (rhombohedral)	P4mm (tetragonal)	Amm2 (orthorhombic)	Cm (monoclinic)	Pm (monoclinic)
As-prepared	9.74 (17.4)	1.46 (6.72)	5.64 (13.2)	3.18 (9.92)	1.16 (5.99)	2.99 (9.64)
Annealed	6.14 (16.1)	1.24 (7.22)	3.57 (12.3)	2.07 (9.35)	1.04 (6.64)	2.05 (9.30)

Downloaded by [Nanjing University] at 21:05 03 May 2015

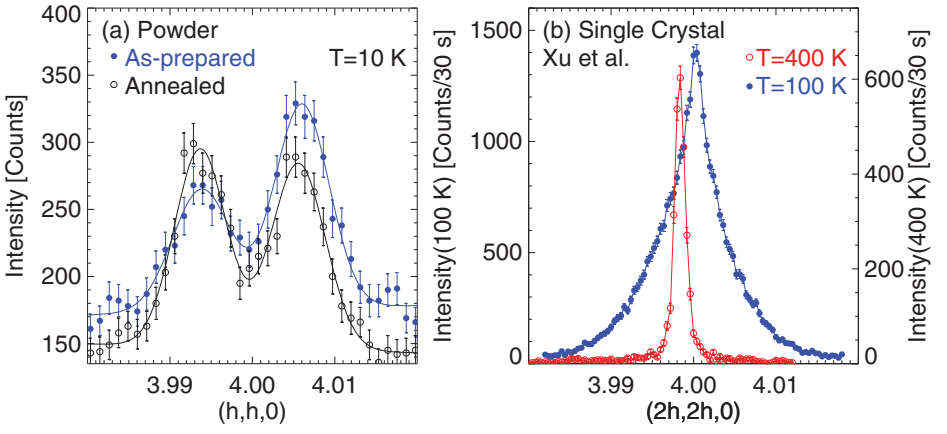


Figure 6. Comparison of Bragg peak profiles for powder and single-crystal samples of PMN-20%PT. (a) The 440_{pc} Bragg peak for the as-prepared and annealed powders as measured with $\lambda = 1.1968$ Å. Solid lines are guides to eye. (b) The 220_{pc} Bragg peak of the single crystal at 100 and 400 K. The x-axis has been multiplied by a factor of two to allow for a direct comparison to the 440_{pc} Bragg peak shown in panel (a).

Radial scans, performed with even greater Q-resolution (1.0×10^{-3} rlu FWHM) of the 220_{pc} Bragg peak of the same PMN-10%PT single crystal were also measured as a function of temperature.[4] Again no splitting of the 220_{pc} peak was observed, but the broadening at lower temperatures is greater than that of the 111_{pc} peak. Also, a large increase of the 220_{pc} peak intensity was observed as the temperature was decreased, particularly below the T_C identified by the powder diffraction measurements. This again highlights the extreme strain-broadening observed at low temperatures, the lack of an observed distortion, and the large release of extinction.

Both the as-prepared and annealed powders of PMN-10%PT exhibit a ground-state symmetry that is lower than cubic. Although the distortion is so small that no clearlyresolved Bragg peaks were observed within the resolution of the BT1 powder diffractometer, the best refinements are consistently obtained assuming *Cm* symmetry. From the resulting atomic displacements, we calculate a polarization that is consistent with the monoclinic M_B structure conjectured by Singh et al. Our refinements also indicate that the distortion is slightly reduced by annealing. The single crystal neutron diffraction measurements on PMN-10%PT are inconsistent with the domain-averaged profile determined from powder refinements of the same composition. Although no explicit splitting of the Bragg reflections is observed, the single crystal diffraction data could be modeled assuming a rhombohedral/monoclinic distortion in which the splitting is hidden by a strain broadening of the Bragg peaks and a highly unequal domain population below T_C. The temperature dependence of the intensity measured at 111_{pc} shows that the crystal undergoes an extreme release of extinction that we believe results from strain induced by the condensation and subsequent growth of locally ordered polar nanoregions followed by a macroscopic phase transition that is localized to the near-surface region.

3.2. Structure of PMN-20%PT

The ground-state structure of PMN-20%PT has been reported as *R*3*m*,[49] *Cm*,[42] or metrically cubic.[2] Both of our as-prepared and annealed PMN-20%PT powders were

Downloaded by [Nanjing University] at 21:05 03 May 2015

Table 4. Refined values of α (R3m) and β (Cm) at 10 K for PMN-20%PT

	$\alpha(^\circ)$	$\beta(^\circ)$	$\alpha(^\circ)$	$\beta(^\circ)$
	$\lambda = 1.5403$ Å	$\lambda = 1.5403$ Å	$\lambda = 1.1968$ Å	$\lambda = 1.1968$ Å
As-prepared	89.812(1)	90.262(2)	89.809(1)	90.269(4)
Annealed	89.825(1)	90.236(5)	89.819(2)	90.252(5)

measured at 10 K on BT-1 with $\lambda = 1.5403$ Å and also $\lambda = 1.1968$ Å, which provides better $\frac{\Delta Q}{Q}$ resolution. The 440_{pc} Bragg peak profiles for the as-prepared and annealed samples obtained from measurements performed at 10 K using $\lambda = 1.1968$ Å are shown in Figure 6 (a). In this case, the 440_{pc} Bragg peaks are clearly and unambiguously split, indicating that both samples are not cubic. The agreement factors for refinement using various models are shown in Table 3. For both powders, the best agreement factors are obtained under *Cm* symmetry.

Table 4 shows the refined values of α and β determined for the as-prepared and annealed samples measured at 10 K on BT-1 using both wavelengths. The refinements

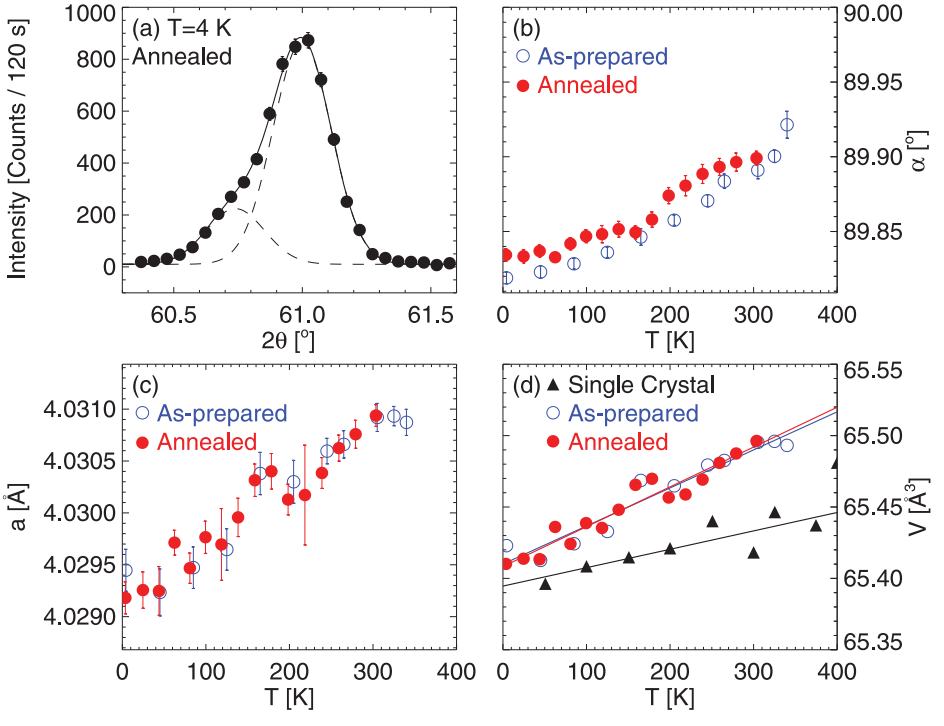


Figure 7. (a) A representative scan through the 111_{pc} Bragg peak of the PMN-20%PT annealed powder sample measured at 4 K on the triple-axis spectrometer BT-9. The total fit, as described in the text, is shown by the solid line. The two individual fitted peaks are shown by dashed lines. (b) Values of α determined from the fit for the annealed and as-prepared samples as a function of temperature. (c) The lattice constant, a, as a function of temperature, determined from the fits. (d) The temperature dependence of the unit cell volume of the two powder samples determined from the fitted values of a and α. Also shown is the thermal expansion of the PMN-20%PT single crystal sample, derived from the values of the lattice constant reported by Xu et al. [2]

Downloaded by [Nanjing University] at 21:05 03 May 2015

again indicate that the annealed sample is slightly less distorted than is the as-prepared sample, which is consistent with the previous finding for PMN-10%PT that annealing after grinding slightly reduces deviations from cubic symmetry.

Neutron scattering measurements of the 220_{pc} Bragg peak from a single crystal of PMN-20%PT with extremely high Q-resolution were reported by Xu et al. and are shown in Figure 6(b) at 100 and 500 K.[2] The horizontal scale has been multiplied by a factor of two to allow for a direct comparison to the 440_{pc} powder peak profiles shown in Figure 6(a). A narrow Gaussian-shaped peak is observed in the cubic phase at high temperature. On cooling, the integrated peak intensity and the peak width were observed to increase, which is consistent with the broadening and release of extinction observed in PMN-10%PT. However, in marked contrast to the powder profiles shown in Figure 6(a), there is no clear splitting of the single-crystal Bragg peak profile at 100 K. Instead the peak profile is well-described by a single broad Lorentzian lineshape. The extreme broadening of the single crystal measurement further indicates that there is a relationship between the size of the crystal and the development of significant strain at lower temperature.

In order to investigate the temperature dependence of the rhombohedral/monoclinic distortion for the powder samples, $\theta - 2\theta$ scans were made through the 111_{pc} Bragg peak for the as-prepared and annealed PMN-20%PT samples between 4 and 340 K on BT-9. A representative scan performed on the annealed powder at 4 K is shown in Figure 7(a), from which a low-angle shoulder due to the rhombohedral distortion is apparent. The scans from both samples were fit to two Gaussian functions constrained to have the same Q-width. The integrated intensity of the larger Gaussian, corresponding to the $11\bar{1}_r$ peak, was constrained to be between three and four times that of the 111_r peak in order to ensure that a reasonable result was achieved; a representative fit is also shown in Figure 7 (a). From the fitting, the rhombohedral unit cell parameters, α and a, were determined as a function of temperature and are shown in Figure 7(b) and 7(c), respectively. The fit of α indicates that for all temperatures the as-prepared sample is slightly more rhombohedrally distorted than is the annealed sample, which supports the finding of the Rietveld refinement discussed above. The lattice parameter a is very similar for the two samples.

The temperature dependence of the unit cell volume for the two powder samples is shown in Figure 7(d). Also shown is the unit cell volume determined from the single crystal neutron scattering measurements reported in [2]. These measurements were fit to a linear equation using data taken below 400 K. The resulting thermal expansion coefficients, α, defined as $\frac{1}{V_0}\frac{dV}{dT}$ where V_0 is the volume at 0 K, were calculated to be 4.1, 4.3, and 2.0×10^{-6} K^{-1} for the as-prepared powder, annealed powder, and the single crystal, respectively. Unusually small thermal expansion coefficients rivaling that of Invar have been noted for the PMN-xPT series.[1,2,4,50] The formation of polar nanoregions near the Burns temperature, which is manifested by the appearance of static (elastic) diffuse scattering just above 400 K, has been suggested as the origin of this effect as the polar nanoregions could then act as a kind of lattice defect that inhibits a normal thermal

Table 5. χ^2 (R_{wp}) for refinements of PMN-30%PT at 10 K.

	$Pm\bar{3}m$ (cubic)	R3m (rhombohedral)	P4mm (tetragonal)	Amm2 (orthorhombic)	Cm (monoclinic)	Pm (monoclinic)
As-prepared	11.1 (15.1)	3.69 (8.71)	4.71 (9.84)	2.96 (7.80)	1.97 (6.36)	2.91 (7.74)
Annealed	12.3 (16.3)	4.21 (9.52)	4.78 (10.2)	6.14 (11.5)	2.00 (6.56)	2.82 (7.79)

Downloaded by [Nanjing University] at 21:05 03 May 2015

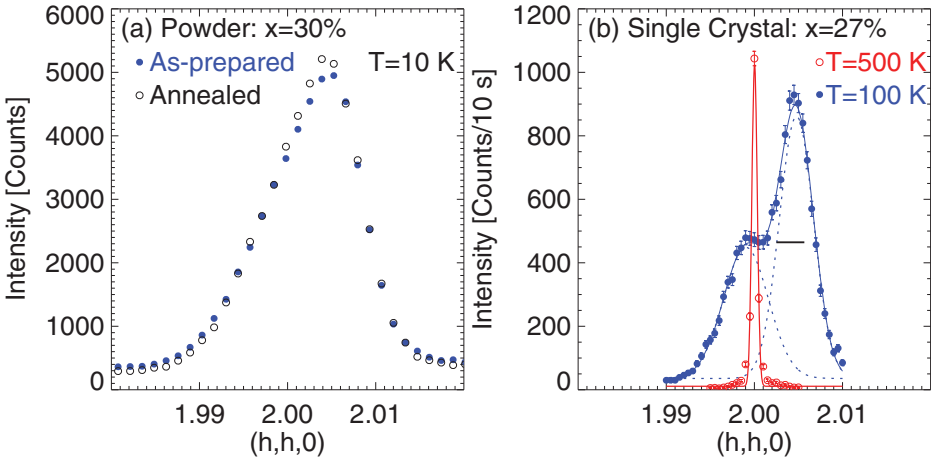


Figure 8. Neutron Bragg peak profiles at 220_{pc} for (a) PMN-30%PT powders at 10 K and (b) single crystal PMN-27%PT at 100 K (blue) and 500 K (red). The powder profiles were measured with $\lambda = 1.5403$ Å. The solid horizontal bar shown in (b) represents the calculated instrumental Q-resolution. Solid lines are guides to the eye.

expansion.[47] This idea is consistent with the fact that above 400 K the polar nanoregions melt (the static diffuse scattering vanishes), at which point the thermal expansion is observed to increase by roughly one order of magnitude.[1,47] The measurements we present here show that both powder samples also display relatively small thermal expansion at low temperatures. However, it is interesting to note that the thermal expansion for the powder samples is roughly twice that for the single crystal. This discrepancy further highlights the fundamentally different behaviors of powder and single-crystal samples of PMN-xPT.

3.3. Structure of PMN-30%PT

Refinements were carried out on the as-prepared and annealed samples of PMN-30%PT using data collected at 10 K and $\lambda = 1.5403$ Å. The agreement factors are given in Table 5. It is evident that the monoclinic (*Cm*) space group yields a much lower value of χ^2 for both samples than does any of the other symmetries. The disparity between the agreement factors for the *Cm* and *R*3*m* phases is also much greater than it is for PMN-10%PT and PMN-20%PT. Thus the PMN-30%PT powder samples are located well within the MPB (*Cm*) region. The refined values of β for the as-prepared and annealed samples at 10 K are 90.246(3)° and 90.234(3)°, respectively, which is again consistent with our findings for PMN-10%PT and PMN-20%PT. We thus conclude that the strain induced by grinding is associated with a larger ferroelectric distortion in PMN-xPT.

Neutron scattering measurements with extremely high Q-resolution, identical to those carried out on single crystals of PMN-xPT with $x = 0.10$ and $x = 0.20$, were also performed on a single crystal PMN-27%PT by Xu et al. [2] Despite the 3% difference between the nominal Ti concentrations, it is instructive to compare the Bragg peak profiles at 220_{pc} for the PMN-30%PT powder samples, shown in panel (a) of Figure 8, to those for single crystal PMN-27%PT, shown in panel (b). The PMN-30%PT powder profiles show a markedly asymmetric lineshape, which is indicative of a structural distortion.

Downloaded by [Nanjing University] at 21:05 03 May 2015

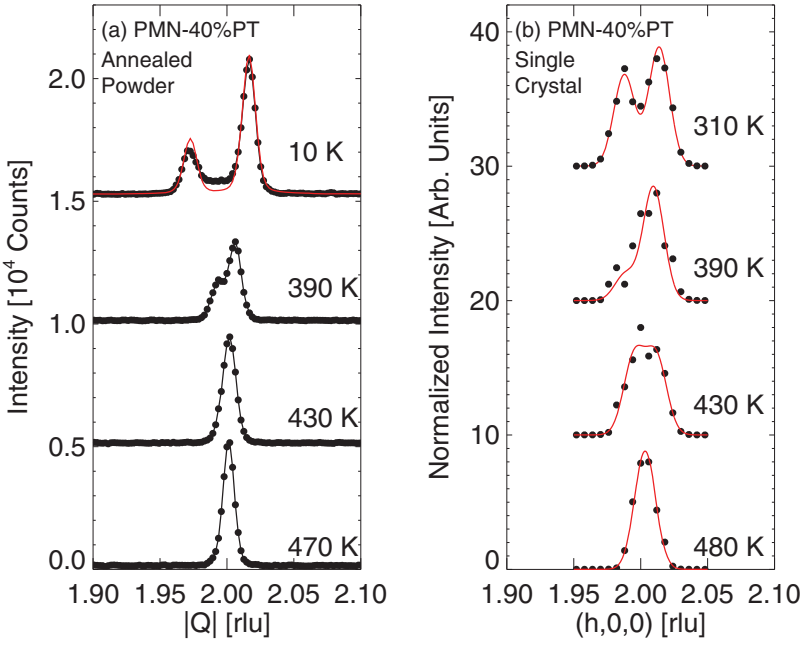


Figure 9. (a) Temperature dependence of the 200_{pc} Bragg peak for the PMN-40%PT annealed powder, which is split by a structural distortion. Under a tetragonal distortion, the peak splits into a doublet (200_t and 002_t). Solid black lines in (a) merely connect data points. The solid red line in (a) represents the calculated intensity assuming tetragonal symmetry ($P4mm$ space group). (b) Radial ($\theta - 2\theta$) scans through the 200_{pc} Bragg peak as a function of temperature for a PMN-40%PT single crystal. The data at 480 K were fit to a single Gaussian function (solid red line), and the data at lower temperatures were fit to two Gaussians, each with a width constrained to be equal to that in the cubic paraelectric phase at 480 K, which we take to represent the instrumental Q-resolution.

The distortion is not as well resolved as that shown for PMN-20%PT in Figure 6(a) because the PMN-20%PT data were obtained at higher $Q = (440)$ using a shorter wavelength of 1.1968 Å. By contrast, the single crystal PMN-27%PT profile, which is resolution-limited at 500 K clearly splits into a doublet on cooling to 100 K. This splitting is not observed for single crystals compositions with $x = 0.10$ or 0.20. Interestingly, the peak lineshape for single crystal PMN-27%PT is measurably broader than the instrumental Q-resolution, which is represented by the horizontal bar. Indeed, the lineshape is so severely strain-broadened that it is impossible to distinguish between monoclinic and rhombohedral symmetries. But more importantly, this indicates that even for $x = 0.27$ the PMN-xPT system still does not attain a long-range ordered, bulk ferroelectric phase on cooling.

3.4. *Structure of PMN-40%PT*

Based on the phase diagrams of Noheda et al. [49] and Singh et al.,[35] we expect the ground state of PMN-40%PT should lie very close to the boundary that separates the monoclinic (Pm) and tetragonal ($P4mm$) phases. Neutron diffraction measurements performed using $\lambda = 1.5403$ Å were performed on both as-prepared and annealed samples at 10 K. These data again support the trend in which smaller distortions are consistently observed for the annealed samples as refinements performed under tetragonal symmetry

Downloaded by [Nanjing University] at 21:05 03 May 2015

yield $c/a = 1.0227$ and 1.0222 for the as-prepared and annealed samples, respectively. Additional data were taken on the annealed sample at 470, 430 , and 390 K for the 002_{pc} peak, and these are shown in panel (a) of Figure 9. At 470 K, the 002_{pc} peak is a narrow singlet, but at 430 K the peak broadens asymmetrically, and at 390 K the peak is clearly split into a doublet. This splitting increases significantly on cooling to 10 K. The gradual splitting of the peak as the temperature is lowered through T_C suggests that the phase transition in PMN-40%PT is second order.

Agreement factors for the monoclinic (*Pm* and *Cm*) and tetragonal (*P*4*mm*) space groups at 10 K are shown in Table 6 (reasonable refinements could not be achieved using rhombohedral or orthorhombic symmetry). All three space groups yield comparable values of agreement, but the best refinement was obtained assuming monoclinic *Pm* symmetry, which agrees with the findings of Singh et al. for PMN-36%PT.[35] We note that the agreement is not as good as that achieved for the refinements of the $x = 0.10$, 0.20, and 0.30 samples. The reason for this poor agreement is largely due to the presence of a substantial amount of unexplained scattering intensity located between several of the split Bragg reflections. This is also illustrated in Figure 9(a), where the intensities calculated from the *P*4*mm* model (shown in red) fail to account for all of the intensity between the split 200_{pc} reflections, which is much larger than predicted. This discrepancy also occurs for refinements using both monoclinic symmetries. The same unexplained scattering is observed in the as-prepared sample. The lack of any well-defined structure between the peaks makes it difficult to decide if there is a co-existing phase that might be contaminating the pattern. An unwanted secondary phase is a possibility given that this composition is located so close to the MPB. Diffuse scattering is another possibility. However, neutron scattering studies of single crystal PMN-40%PT [51] and PMN-60%PT [36] have shown that there is no diffuse scattering below T_C on the tetragonal side of the MPB boundary; thus, we believe that this additional intensity must have some other origin.

Finally, we compare our neutron powder diffraction measurements on PMN-40%PT to radial line scans measured on a single crystal of the same nominal composition. The value of T_C for the single crystal was determined to be 440 K $\pm$ 1 K based on the strong release of extinction measured at the 200 Bragg peak. As shown in panel (b) of Figure 9, the single crystal 200_{pc} Bragg peak profile is well described by a resolution-limited Gaussian lineshape (shown in red) in the cubic phase at 480 K. On cooling to 430 K, the profile broadens significantly and appears to split; this is consistent with the broadening we observe in the powder sample at the same temperature. On cooling to 310 K, the profile is clearly split and well described by two resolution-limited Gaussians. This indicates that the single crystal undergoes a well-defined, long-range ordered phase transition, which is not the case for single crystals of PMN-10%PT, PMN-20%PT, and PMN-27%PT. This finding, coupled with that of Stock et al. for single crystal PMN-60%PT, [36] which also exhibits a well-defined, long-range ordered structural phase transition, is important because it suggests that the skin effect vanishes for PMN-*x*PT compositions located on the tetragonal side of the MPB.

Table 6. χ^2 (R_{wp}) for refinements of PMN-40%PT at 10 K.

	$Pm\bar{3}m$ (cubic)	R3m (rhombohedral)	P4mm (tetragonal)	Amm2 (orthorhombic)	C1m1 (monoclinic)	P1m1 (monoclinic)
As-prepared	—	—	2.75 (8.22)	—	2.62 (8.03)	2.52 (7.85)
Annealed	—	—	3.52 (8.77)	—	3.52 (8.77)	3.37 (8.57)

Downloaded by [Nanjing University] at 21:05 03 May 2015

Downloaded by [Nanjing University] at 21:05 03 May 2015

4. Discussion and conclusions

The PMN-xPT system exhibits complicated structures that are composed of a long-range ordered matrix and local, polar deviations from this matrix. The neutron scattering data we present here demonstrate that the long-range (average) structures of single crystal and powder specimens of PMN-xPT differ intrinsically from one another and that these differences depend on the Ti concentration x. The Bragg peak profiles measured on single crystal samples with $x = 0.10$, 0.20, and 0.27 are not consistent with the structures determined from Rietveld refinements of neutron powder diffraction patterns obtained from samples with similar compositions. Whereas powder samples with $x > 0$ undergo long-range ordered phase transitions to lower, polar symmetries on cooling, single crystal samples on the Ti-poor side of the MPB do not. Instead single crystals of PMN-xPT either become highly strained and remain metrically cubic ($a = b = c$ and $\alpha = \beta = \gamma = 90^\circ$) at low temperatures for $x \leq 0.20$, or they exhibit short-range, pseudo-rhombohedral, polar distortions for $0.20 < x \approx 0.27$. We do find agreement between powder and single crystal neutron diffraction measurements for $x = 0.40$, i. e. on the tetragonal side of the MPB. These results are summarized in Figure 10, which displays a schematic phase diagram for PMN-xPT in which the phase boundaries are based on the dielectric permittivity and piezo-resonance frequency data of Singh et al.[35] The color in Figure 10 reflects the crystal symmetry: near $x = 0$ it gradually fades to white to represent the fact that PMN (and probably a narrow range of compositions near $x = 0$) retains a cubic phase at all temperatures. For intermediate compositions, the color is uniformly green to indicate that powders exhibit *Cm* symmetry while single crystals remain metrically cubic. Close to the MPB the color changes from green to blue to highlight the fact that single crystal compositions with $x > 0.20$ exhibit short-range order that is likely rhombohedral or monoclinic in nature. The precise concentration x_c at which the skin effect vanishes is unknown, but from the data presented here we know that it lies in the range $0.27 < x_c < 0.40$, which brackets the MPB region. On this point, the neutron diffraction study of single crystal PMN-32%PT by Wen et al.[52] is of particular importance because it reports changes in the linewidths of the 300_{pc} Bragg peak on cooling at temperatures that are consistent with the phase diagram of Singh et al.[35] Based on the study by Wen et al., we *speculate* that $x_c \approx 0.31$, i. e. that the skin effect vanishes at or near the boundary between the *Cm* and

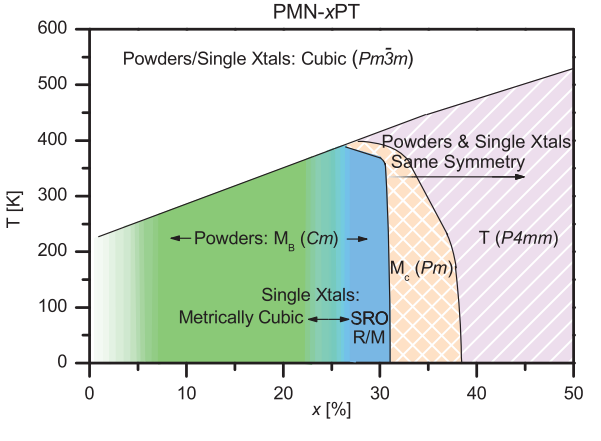


Figure 10. Schematic phase diagram for PMN-xPT. 'SRO R/M' stands for short-range order that is likely rhombohedral or monoclinic. The phase boundaries are taken from Singh et al. [35]

Pm phases. This is indicated in Figure 10 as the point where the structures of powder and single crystal specimens of PMN-*x*PT coincide.

Our neutron scattering data also demonstrate that as-prepared powder samples that are subsequently annealed in air at 873 K for 2 h consistently exhibit smaller structural distortions on cooling than do those that have not been annealed. Based on this result, we can predict that if the near-surface region or skin of a single crystal is more strained than is the bulk, then the ferroelectric distortions should be larger in the skin. In fact, the combined results of Conlon et al. on PMN [3] and Xu et al. on PZN-*x*PT [8] suggest this to be the case, and in this respect our results here correlate well with the skin effect. But as shown in Table 4 and panel (b) of Figure 7, the differences between the distortions in as-prepared and annealed samples are extremely small. Moreover the annealed samples (nominal zero strain) always distort on cooling independent of composition, which is not true for bulk single crystals. For these reasons, we believe that *mechanically induced* strain, such as irreversible plastic deformations produced by grinding or polishing, and/or oxygen vacancies are not viable explanations for the skin effect. The result that grinding produces slightly larger distortions in PMN-*x*PT may seem obvious given its piezoelectric character, but grinding does not always have this effect. A synchrotron study of the structural phase transitions and thermal expansion in several single crystal compositions of $KTa_{1-x}Nb_xO_3$ (KTN) by Gehring et al. reported the presence of three ferroelectric transitions for $x = 0.157$ that were identified via the splitting of the 420_{pc} Bragg peak on cooling. However, when a small piece of this crystal was broken off and powdered and the measurement repeated, no structural distortions of any sort were observed down to 21 K. [53] This surprising result was suggested to be due to either the presence of a finite-strain-field effect, which has been observed in KCN,[54] or a strong finite-particle-size effect, which has been reported in $BaTiO_3$.[55]

From the data presented in panels (c) and (d) in Figure 7, we see that the rates of thermal expansion are different between single crystal and powder samples of the same composition, whereas any differences in the thermal expansion between as-prepared and annealed samples are either absent or too small for us to detect. Specifically, the $x = 0.20$ powder samples exhibit an average coefficient of thermal expansion of 4.2×10^{-6} K^{-1} below 400 K, which is twice that of the $x = 0.20$ single crystal (2.0×10^{-6} K^{-1}). Previous X-ray studies of ceramic PMN-*x*PT by King et al. reported thermal expansion coefficients between 300 and 400 K of 3×10^{-6} K^{-1} for $x = 0.10$,[56] and 1×10^{-6} K^{-1} for $x = 0.20$. [57] Given the smaller temperature range of the X-ray studies, we consider these values to be in reasonably good agreement with our neutron results. In addition, both X-ray and neutron studies agree that above 400 K the coefficients of thermal expansion of both powders and single crystals of PMN-*x*PT increase by roughly one order of magnitude. As mentioned earlier, this increase has been suggested to be related to the melting of the polar nanoregions (elastic diffuse scattering) in PMN-*x*PT, and in fact a similar increase has been documented with X-ray scattering in many other lead-based relaxors by Dkhil et al. at similar temperatures.[58] The question remains, however, as to why powders and single crystals of the same composition exhibit different thermal expansion coefficients. Assuming that the proposed explanation for the Invar-like rates of thermal expansion in the presence of static diffuse scattering is correct, we speculate that the answer is because the density of polar nanoregions is lower in the skin region than it is in the bulk. If correct, then the diffuse scattering intensity should be weaker in the skin region than it is in the bulk. Experimental support for this idea comes from X-ray measurements by Dkhil et al., which preferentially probe the near-surface region, on single crystal samples of PMN-*x*PT with $x = 0.25$ and $x = 0.30$ that show almost no evidence of the diffuse

Downloaded by [Nanjing University] at 21:05 03 May 2015

scattering that is easily observed with neutron scattering methods for compositions up to $x = 0.32$.[52, 59] To the extent that they inhibit thermal expansion, a lower density of polar nanoregions in powder samples would be consistent with the higher thermal expansion coefficients reported here. This would also be consistent with an expanded skin effect concept in which both long-range and short-range structural differences exist between the near-surface region and the bulk of single crystals.

Stock et al.[5,26,36] have conjectured that the origin of the skin effect is connected to the presence of random fields insofar as the situation in relaxors is analogous to case of the random-field Ising antiferromagnet $Mn_{0.5}Zn_{0.5}F_2$ for which long-range magnetic order is observed via X-ray diffraction, but only short-range magnetic order is observed via neutron diffraction.[37] They reasoned that the relaxor problem can be mapped onto to a three-dimensional system of Heisenberg spins in the presence of a cubic anisotropy and an isotropic random magnetic field where, following a suggestion of Aharony, [60] the Hamiltonian $H = H_{\text{Heis}} + H_{RF} + H_{\text{Cubic}}$ is such that $H_{\text{Heis}} > H_{RF} > H_{\text{Cubic}}$. At temperatures sufficiently high to render the cubic anisotropy negligible, the system will behave as a Heisenberg magnet in the presence of a random field. The ordered state of such a system is wellknown to be unstable against arbitrarily small random fields in less than four dimensions, thus the system will break up into domains (i. e. polar nanoregions) below the ordering temperature of the bare Heisenberg system.[61] On cooling to temperatures where the cubic anisotropy becomes important, the system will begin to behave more like an Ising system, which exhibits long-range order in the presence of sufficiently small random fields.[62] Our findings here establish an upper compositional bound of $x_c < 0.40$ on the skin effect, which together with the neutron study of Wen et al. on PMN-32%PT implies that the skin effect vanishes very close to (or within) the MPB. This suggests that there is an important balance between the energetics of the ferroelectric distortion and the strength of the REFs, both of which depend on the composition x, that exhibits a crossover within the MPB region. In the context of the random-field picture of Stock et al., given that the random field term H_{RF} necessarily decreases with increasing x, then assuming only that the cubic anisotropy term H_{Cubic} varies less rapidly one must eventually obtain the situation where $H_{\text{Heis}} > H_{\text{Cubic}} > H_{RF}$. In this case, one recovers the properties of an Ising system in a random field, which exhibits true long-range order and no domains. Thus the vanishing of the skin effect is likely less dependent on crystal symmetry and more dependent on the weakening of the REF strength. Our findings on PMN-40%PT and those of Stock et al.[36] on PMN-60%PT indicate that this picture accurately describes PMN-xPT on the tetragonal side of the MPB and possibly into the Pm region of the MPB. The fact that the neutron elastic diffuse scattering, relaxor properties, and exceptional piezoelectric character of PMN-xPT also vanish near the MPB suggest that they too may be related to REFs and intimately connected to the skin effect. We hope that these results will stimulate further theoretical research in this area.

Acknowledgements

The authors acknowledge useful discussions with J. K. Stalick and S. Ji as well as the support of the National Institute of Standards and Technology, US Department of Commerce, in providing the neutron research facilities used in this work.

Disclosure statement

No potential conflict of interest was reported by the authors.

Downloaded by [Nanjing University] at 21:05 03 May 2015

Funding

The work at Simon Fraser University was supported by the United States Office of Naval Research (ONR) [grant number N00014-12-1-1045]; the Natural Sciences and Engineering Research Council of Canada (NSERC) [grant number 203772]. Work in the Materials Science Division at Argonne National Laboratory is supported by the US Department of Energy, Office of Science, Basic Energy Sciences, Materials Science and Engineering Division [grant number DE-AC02-06CH11357]. G. Xu acknowledges support from the Office of Basic Energy Sciences, US Department of Energy [grant number DE-AC02-98CH10886], while C. Stock acknowledges the Carnegie Trust for the Universities of Scotland and the Royal Society.

References

[1] Gehring PM, Chen W, Ye ZG, Shirane G. The non-rhombohedral low-temperature structure of PMN-10%PT. J Phys: Condens Matter. 2004; 16: 7113−7121.
[2] Xu G, Viehland D, Li JF, Gehring PM, Shirane, G,. Evidence of decoupled lattice distortion and ferroelectric polarization in the relaxor system PMN-*x*PT. Phys Rev B. 2003; 68: 212410.
[3] Conlon KH, Luo H, Viehland D, Li JF, Whan T, Fox JH, Stock C, Shirane G. Direct observation of the near-surface layer in $Pb(Mg_{1/3}Nb_{2/3})O_3$ using neutron diffraction. Phys Rev B. 2004; 70: 172204.
[4] Xu G, Gehring PM, Stock C, Conlon K. The anomalous skin effect in single crystal relaxor ferroelectric PZN-*x*PT and PMN-*x*PT. Phase Transitions. 2006; 79: 135−152.
[5] Stock C, Xu G, Gehring PM, Luo H, Zhao X, Cao H, Li JF, Viehland D, Shirane G. Neutron and x-ray diffraction study of cubic [111] field-cooled $Pb(Mg_{1/3}Nb_{2/3})O_3$. Phys Rev B. 2007; 76: 064122.
[6] Xu G, Zhong Z, Bing Y, Ye ZG, Stock C, Shirane G. Ground state of the relaxor ferroelectric $Pb(Zn_{1/3}Nb_{2/3})O_3$. Phys Rev B. 2003; 67: 104102.
[7] Xu G, Zhong Z, Bing Y, Ye ZG, Stock C, Shirane G. Anomalous phase in the relaxor ferroelectric $Pb(Zn_{1/3}Nb_{2/3})O_3$. Phys Rev B. 2004; 70: 064107.
[8] Xu G, Hiraka H, Shirane G, Ohwada K. Dual structures in $(1-x)Pb(Zn_{1/3}Nb_{2/3})O_3$-$xPbTiO_3$ ferroelectric relaxors. App Phys Lett. 2004; 84: 3975−3977.
[9] Park SE, Shrout TR. Ultrahigh strain and piezoelectric behavior in relaxor based ferroelectric single crystals. J Appl Phys. 1997; 82: 1804−1811.
[10] Kuwata J, Uchino K, Nomura S. Dielectric and piezoelectric properties of $0.91Pb(Zn_{1/3}Nb_{2/3})O_3$-$0.09PbTiO_3$ single crystals. Jpn J Appl Phys. 1982; 21: 1298−1302.
[11] Uchino K. Ferroelectric devices. New York: Marcel Dekker; 2000.
[12] Ye ZG. Relaxor ferroelectric complex perovskites: structure, properties and phase transitions. Key Eng Mater. 1998; 155-156: 81−122.
[13] Cowley RA, Gvasaliya SN, Lushnikov SG, Roessli B, Rotaru GM. Relaxing with relaxors: a review of relaxor ferroelectrics. Adv Phys. 2011; 60: 229−327.
[14] Davis M. Picturing the elephant: giant piezoelectric activity and the monoclinic phases of relaxor-ferroelectric single crystals. J Electroceram. 2007; 19: 23−45.
[15] Ohwada K, Hirota K, Rehrig PW, Fuji Y, Shirane G. Neutron diffraction study of field-cooling effects on the relaxor ferroelectric $Pb[(Zn_{1/3}Nb_{2/3})_{0.92}Ti_{0.08}]O_3$. Phys Rev B. 2003; 67: 094111.
[16] Kuwata J, Uchino K, Nomura S. Phase transitions in the $Pb(Zn_{1/3}Nb_{2/3})O_3$-$PbTiO_3$ system. Ferroelectrics. 1981; 37: 579−582.
[17] Lebon A, Dammak H, Calvarin G, Ahmedou IO. The cubic-to-rhombohedral phase transition of $Pb(Zn_{1/3}Nb_{2/3})O_3$: a high-resolution x-ray diffraction study on single crystals. J Phys: Condens Matter. 2002; 14: 7035−7043.
[18] Thurston TR, Helgesen G, Gibbs D, Hill JP, Gaulin BD, Shirane G. Observation of 2 length scales in the magnetic critical fluctuations of holmium. Phys Rev Lett. 1993; 70: 3151−3154.
[19] Gehring PM, Hirota K, Majkrzak CF, Shirane G. Origin of the 2nd length scale above the magnetic-spiral phase of Tb. Phys Rev Lett. 1993; 71: 1087−1090.
[20] Hirota K, Shirane G, Gehring PM, Majkrzak CF. Neutron-scattering studies of the 2 magnetic correlation lengths in terbium. Phys Rev B. 1994; 49: 11967−11978.
[21] Gehring PM, Hirota K, Majkrzak CF, Shirane G. Absence of the anomalous 2nd length scale in the bulk of terbium single-crystal. Phys Rev B. 1995; 51: 3234−3237.

Downloaded by [Nanjing University] at 21:05 03 May 2015

[22] Shirane G, Cowley RA, Matsuda M, Shapiro SM. q dependence of the central peak in the inelastic-neutron-scattering spectrum of $SrTiO_3$. Phys Rev B. 1993; 48: 15595−15602.
[23] Rütt U, Diederichs A, Strempfer J, Schneider JR, Shirane G. Depth dependence of strain, mosaicity and sharp component in the critical scattering of $SrTiO_3$. Europhys Lett. 1997;39:395−400; Europhys Lett. 40:235.
[24] Martí X, Ferrer P, Herrero-Albillos J, Narvaez J, Holy V, Barrett N, Alexe M, Catalan G. Skin layer of $BiFeO_3$ single crystals. Phys Rev Lett. 2011; 106: 236101.
[25] Fujishiro K, Iwase T, Uesu Y, Yamada Y, Dkhil B, Kiat J-M, Mori S, Yamamoto N. Optical and structural studies of long-range order development in relaxor ferroelectrics. J Phys Soc Jpn. 2000; 69: 2331−2338.
[26] Stock C, Birgeneau RJ, Wakimoto S, Gardner JS, Chen W, Ye ZG, Shirane G. Universal static and dynamic properties of the structural transition in $Pb(Zn_{1/3}Nb_{2/3})O_3$. Phys Rev B. 2004; 69: 094104.
[27] Kisi EH, Forrester JS. Crystal structure of the relaxor ferroelectric PZN: demise of the 'X-phase'. J Phys: Condens Matter. 2005; 17: L381−L384.
[28] Kisi EH, Forrester JS, Howard CJ, Ibberson RM. Search for the X-phase in poled PZN-PT using very high-resolution single-crystal neutron diffraction. J Phys: Condens Matter. 2007; 19: 232201.
[29] Forrester JS, Kisi EH, Knight KS, Howard CJ. Rhombohedral to cubic phase transition in the relaxor ferroelectric PZN. J Phys: Condens Matter. 2006; 18: L233−L240.
[30] Xu G, Viehland D, Li JF, Gehring PM, Shirane G. Evidence of decoupled lattice distortion and ferroelectric polarization in the relaxor system PMN-xPT. Phys Rev B. 2003; 68: 212410.
[31] Dkhil B, Kiat JM, Calvarin G, Baldinozzi G, Vakhrushev SB, Suard E. Local and long range polar order in the relaxor-ferroelectric compounds $PbMg_{1/3}Nb_{2/3}O_3$ and $PbMg_{0.3}Nb_{0.6}Ti_{0.1}O_3$. Phys Rev B. 2001; 65: 024104.
[32] Ye ZG, Bing Y, Gao J, Bokov AA, Stephens P, Noheda B, Shirane G. Development of ferroelectric order in relaxor $(1-x)Pb(Mg_{1/3}Nb_{2/3})O_3$-$x$$PbTiO_3$ $(0\leq x\leq 0.15)$. Phys Rev B. 2003; 67: 104104.
[33] Bonneau P, Garnier P, Husson E, Morell A. Structural study of PMN ceramics by x-ray diffraction between 297 and 1023 K. Mat Res Bull. 1989; 24: 201.
[34] de Mathan N, Husson E, Calvarin G, Gavarri JR, Hewat AW, Morell A. A structural model for the relaxor $PbMg_{1/3}Nb_{2/3}O_3$ at 5 K. J Phys: Condens Matter. 1991; 3: 8159−8171.
[35] Singh AK, Pandey D, Zaharko O. Powder neutron diffraction study of phase transitions in and a phase diagram of $(1-x)[Pb(Mg_{1/3}Nb_{2/3})O_3]$-$x$$PbTiO_3$. Phys Rev B. 2006; 74: 024101.
[36] Stock C, Ellis D, Swainson IP, Xu G, Hiraka H, Zhong Z, Luo H, Zhao X, Viehland D, Birgeneau RJ, Shirane G. Damped soft phonons and diffuse scattering in $40\%Pb(Mg_{1/3}Nb_{2/3})O_3$-$60\%PbTiO_3$. Phys Rev B. 2006; 73: 064107.
[37] Hill JP, Thurston TR, Erwin RW, Ramstad MJ, Birgeneau RJ. Transition to long-range order in the three-dimensional random-field Ising model. Phys Rev Lett. 1991; 66: 3281−3284.
[38] Stalick JK, Prince E, Santoro A, Schroder IG, Rush JJ. Materials science applications of the new National Institute of Standards and Technology powder diffractometer. Mater Res Soc Proc. 1994; 376: 101−106.
[39] Larson AC, Von Dreele RB. General Structure Analysis System (GSAS); 2004. (Los Alamos National Laboratory Report; LAUR 86-748).
[40] Toby BH. EXPGUI, a graphical user interface for GSAS. J Appl Cryst. 2001; 34: 210−213.
[41] Corker DL, Glazer AM, Whatmore RW, Stallard A, Fauth F. A neutron diffraction investigation into the rhombohedral phases of the perovskite series PbZr1-xTixO3. J Phys: Condens Matter. 1998; 10: 6251.
[42] Singh AK, Pandey P, Zaharko O. Evolution of short-range to long-range monoclinic order of M_B type with decreasing temperature in $0.75[Pb(Mg_{1/3}Nb_{2/3})O_3]$-$0.25PbTiO_3$. J Appl Phys. 2006; 99: 076105.
[43] Carreaud J, Kiat JM, Dkhil B, Alguero M, Ricote J, Jimenez R, Holc J, Kosec M. Monoclinic morphotropic phase and grain size-induced polarization rotation in $Pb(Mg_{1/3}Nb_{2/3})O_3$ − $PbTiO_3$. Appl Phys Lett. 2006; 89: 252906.
[44] Le Bail A, Druoy H, Fourquet JL. Ab-initio structure determination of $LiSbWO_6$ by X-ray powder diffraction. Mater Res Bull. 1988; 23: 447−452.
[45] Stephens P. Phenomenological model of anisotropic peak broadening in powder diffraction. J Appl Cryst. 1999; 32: 281−289.

Downloaded by [Nanjing University] at 21:05 03 May 2015

[46] Xu G, Gehring PM, Ghosh VJ, Shirane G. High-*q*-resolution neutron scattering technique using triple-axis spectrometers. Acta Cryst. 2004; A60: 598−603.
[47] Gehring PM, Hiraka H, Stock C, Lee SH, Chen W, Ye ZG, Vakhrushev SB, Chowdhuri Z. Reassessment of the Burns temperature and its relationship to the diffuse scattering, lattice dynamics, and thermal expansion in relaxor $Pb(Mg_{1/3}Nb_{2/3})O_3$. Phys Rev B. 2009; 79: 224109.
[48] Stock C, Van Eijck L, Fouquet P, Maccarini M, Gehring PN, Xu G, Luo H, Zhao X, Li JF, Viehland D. Interplay between static and dynamic polar correlations in relaxor Pb $(Mg_{1/3}Nb_{2/3})O_3$. Phys Rev B. 2010; 81: 144127.
[49] Noheda B, Cox DE, Shirane G, Gao J, Ye ZG. Phase diagram of the ferroelectric relaxor $(1-x)Pb(Mg_{1/3}Nb_{2/3})O_3$-$x$$PbTiO_3$. Phys Rev B. 2002; 66: 054104.
[50] Zhao J, Glazounov AE, Zhang QM, Toby B. Neutron diffraction study of electrostrictive coefficients of prototype cubic phase of relaxor ferroelectric $PbMg_{1/3}Nb_{2/3}O_3$. Appl Phys Lett. 1998; 72: 1048−1050.
[51] Matsuura M, Hirota K, Gehring PM, Ye ZG, Chen W, Shirane G. Composition dependence of the diffuse scattering in the relaxor ferroelectric compound $(1-x)Pb(Mg_{1/3}Nb_{2/3})O_3$-$x$$PbTiO_3$ $(0\leq x\leq 0.40)$. Phys Rev B. 2006; 74: 144107.
[52] Wen J, Xu G, Stock C, Gehring PM. Response of polar nanoregions in 68%$Pb(Mg_{1/3}Nb_{2/3})O_3$-32%$PbTiO_3$ to a [001] electric field. Appl Phys Lett. 2008; 93: 082901.
[53] Gehring PM, Chou H, Shapiro SM, Hriljac JA, Chen DH, Toulouse J, Rytz D, Boatner LA. Dipole-glass behavior of lightly-doped $KTa1-xNb_xO_3$. Phys Rev B. 1992; 46: 5116.
[54] Knorr K. Random-strain-field effects on the low-temperature state of KCN. Phys Rev Lett. 1991; 66: 3016.
[55] Uchino K, Sadanaga E, Hirose T. Dependence of the crystal structure on particle size in barium titanate. J Am Ceram Soc. 1989; 72: 1555.
[56] King HW, Yildiz M, Ferguson SH, Waechter DF, Prasad SE. X-ray measurement of thermal expansion in electrostrictive 0.9PMN-0.1PT. Ferro Lett. 2004; 31: 55.
[57] King HW, Ferguson SH, Waechter DF, Prasad SE. An x-ray diffraction study of PMN-PT ceramics near the morphotropic phase boundary. In: Sastry, HRS, Ebenezer, DD, and Sundaram, TVS, editors. Proceedings of ICONS 2002, International Conference on Solar-Sensors Systems; 2002. p. 677−685.
[58] Dkhil B, Gemeiner P, Al-Barakaty A, Bellaiche L, Dul'kin E, Mojaev E, Roth M. Intermediate temperature scale T^* in lead-based relaxor systems. Phys Rev B. 2009; 80: 064103.
[59] Dkhil, B and Vakhrushev, S. Private communication.
[60] Aharony, A. Private communication.
[61] Imry Y, Ma SK. Random-field instability of the ordered state of continuous symmetry. Phys Rev Lett. 1975; 35: 1399.
[62] Bricmont J, Kupiainen A. Lower critical dimension for the random-field Ising model. Phys Rev Lett. 1987; 59: 1829.

Downloaded by [Nanjing University] at 21:05 03 May 2015